International Journal of Minerals, Metallurgy and Materials
Volume 25, Number 1, January 2018, Page 73
https://doi.org/10.1007/s12613-018-1548-0

Preparation of nano-TiO_2/diatomite-based porous ceramics and their photocatalytic kinetics for formaldehyde degradation

Ru-qin Gao[1)], *Qian Sun*[1)], *Zhi Fang*[2)], *Guo-ting Li*[1)], *Meng-zhe Jia*[1)], *and Xin-mei Hou*[2)]

1) School of Environmental Science and Engineering, North China University of Water Resources and Electric Power, Zhengzhou 450011, China
2) Collaborative Innovation Center of Steel Technology, University of Science and Technology Beijing, Beijing 100083, China
(Received: 24 May 2017; revised: 11 July 2017; accepted: 17 July 2017)

Abstract: Diatomite-based porous ceramics were adopted as carriers to immobilize nano-TiO_2 via a hydrolysis-deposition technique. The thermal degradation of as-prepared composites was investigated using thermogravimetric–differential thermal analysis, and the phase and microstructure were characterized by X-ray diffraction, Fourier transform infrared spectroscopy, and transmission electron microscopy. The results indicated that the carriers were encapsulated by nano-TiO_2 with a thickness of 300–450 nm. The main crystalline phase of TiO_2 calcined at 650°C was anatase, and the average grain size was 8.3 nm. The FT-IR absorption bands at 955.38 cm^{-1} suggested that new chemical bonds among Ti, O, and Si had formed in the composites. The photocatalytic (PC) activity of the composites was investigated under UV irradiation. Furthermore, the photodegradation kinetics of formaldehyde was investigated using the composites as the cores of an air cleaner. A kinetics study showed that the reaction rate constants of the gas-phase PC reaction of formaldehyde were $\kappa = 0.576$ mg·m^{-3}·min^{-1} and $K = 0.048$ m^3/mg.

Keywords: nano titanium dioxide/diatomite; porous ceramics; hydrolysis precipitation; photocatalytic activity; kinetic equation; formaldehyde degradation

1. Introduction

With the improvement of living standards and the enhancement of environmental consciousness, the requirements for higher indoor environmental quality have become an urgent need for every citizen. Indoor air purification has become an urgent problem. Formaldehyde is the main chemical responsible for indoor air pollution and has been shown to be a serious threat to people's healthy. However, traditional methods for adsorption or chemical degradation of formaldehyde are ineffective or result in secondary pollution. Hence, the development of an economical and efficient technique for the reduction of formaldehyde is urgently needed. Photocatalysis is an environmental friendly technology that has attracted much attention for its potential application in the degradation of various environmental pollutants [1–4]. Photocatalysis oxidation technology is an emergent environmental pollution treatment technology in which various metal oxides (i.e., TiO_2, ZnO, MoO_3, CeO_2, ZrO_2, WO_3, α-Fe_2O_3, and SnO_2) and metal sulfides (i.e., ZnS, CdS, WS_2, and MoS_2) are used as catalysts because of their electronic structure, which is characterized by a filled valence band and an empty conduction band. In this regard, nano-TiO_2 is well known for its photocatalytic (PC) properties, which include a high oxidizing power, as well as its nontoxicity and long-term photostability. Various TiO_2 crystalline phases, including anatase, rutile, and brookite [5–8], have been used in different fields because of their superior photodegradation performance of various environmental pollutants in both gaseous and liquid phases [9–11]. Unfortunately, the aggregation of nano-TiO_2 and the difficulty in regenerating it often limit its practical application. Therefore, titanium oxide coatings on larger cores have been investigated to coat TiO_2 onto carriers with high specific surface areas. This approach can not only prevent aggregation of fine-TiO_2 powder particles but also lead to high photodecomposition performance [12].

In recent years, various porous materials, including por-

Corresponding author: Ru-qin Gao E-mail: 15838335721@163.com; Xin-mei Hou E-mail: houxinmeiustb@ustb.edu.cn

ous glass beads, synthetic molecular sieves, activated carbon, zeolites, and various synthetic materials [13–16], have been used as carriers for nano-TiO_2. The biggest advantage of these materials as carriers is that they have a larger specific surface area, which actually increases the local concentration of organics and avoids the volatilization or dissociation of the intermediates. The reaction rate is accelerated accordingly [17–18].

Diatomite is a siliceous rock composed of remnants of algae and other microorganisms. The relative density of pure, dry diatomite is 0.4–0.9 g/cm^3, and the pore size distribution is 50–800 nm [19–20]. Diatomite-based porous ceramic (DBPC) can combine the original pore structure of the diatomite with the holes accumulated by aggregating particles. As a result, DBPC has recently been attracting increasing attention.

In this study, nano-TiO_2/DBPC composites were synthesized through a typical hydrolysis precipitation process in which $TiCl_4$ was used as a precursor. The PC activity was investigated by the PC degradation of formaldehyde under UV irradiation. On the basis of the results, the kinetic equations of photocatalysis were established.

2. Material and methods

2.1. Preparation of diatomite-based porous ceramics coated with the nano-TiO_2 thin film

Diatomite (North Diatomite Co., China) with a pore diameter of 50–800 nm and a specific surface area of 19.88 m^2/g was used in the experiments. The main chemical components were as follows: SiO_2, 82.62wt%; Al_2O_3, 4.76wt%; Fe_2O_3, 2.01wt%. Sintering aids, including feldspar, quartz, and kaolin were used as raw materials to prepare DBPC. The powders were mixed, milled, molded, and then calcined at 980°C (2 h) to prepare the carrier of DBPC with dimensions of ϕ115 mm × 3 mm. The burned ceramic chips were cleaned ultrasonically in distilled water three times and dried at 105°C.

Hydrated TiO_2 was loaded onto the surface of DBCP by the following process: DBPC and distilled water with a molar ratio of 1:22 were placed in a beaker at 5°C in an ice-water bath. Under vigorous stirring, $TiCl_4$ (2.9 mol/L, synthetic grade, Beijing Yili Fine Chemicals Co., China) was added dropwise to the beaker using a constant flow pump and the resultant mixture was stirred for 15 min. A mixture of ammonium sulfate (1.5 mol/L, synthetic grade, Beijing Yili Fine Chemicals Co., China) and concentrated hydrochloric acid were pumped into the beaker. The pH value of the aforementioned solution was adjusted to 5.0; the solution was then heated to 50°C and maintained at this temperature for 1 h. The white precipitate was collected on filter paper, washed several times with deionized water, and dried. Nano-TiO_2/DBPC samples as cores were obtained by drying at 105°C and were subsequently treated at various temperatures for 2 h.

2.2. Sample characterization

The reaction process was characterized by thermogravimetry–differential thermal analysis (TG–DTA, model STA 499C, Netzsch, Germany) over the temperature range from 20 to 1100°C at a heating rate of 20°C/min in air. The crystal structure of the samples was characterized by X-ray diffraction (XRD, X'Pert, The Netherlands; tube voltage: 40 kV; tube electric current: 40 mA; Cu target; length of stride: λ = 0.15406 nm; scanning angle (2θ): 10° to 80°; scanning speed: 0.01°/s). The structure and organization of the samples were determined by Fourier transform infrared spectroscopy (FT-IR, BIO-RAD FTS 3000, USA). The sample calcined at 650°C was used to observe the cross-section morphology of the nanometric TiO_2. The surface morphology of the sample was observed by transmission electron microscopy (TEM) using a JEOL 2100 electron microscope.

2.3. PC activity of samples

A schematic of the PC test for formaldehyde is shown in Fig. 1. The PC activity experiments were carried out in accordance with standard GB 50325—2001. The system consists of two environmental chambers and one air purifier. The power and wavelength of the ultraviolet (UV) source were 8 W and 365 nm, respectively. A small electric fan was installed at the purifier air inlet to ensure that air could flow into the two environmental chambers.

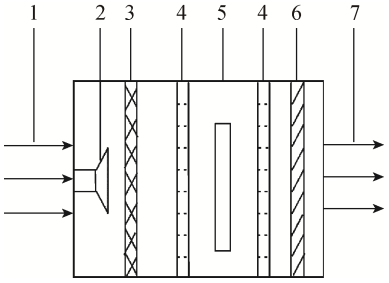

Fig. 1. Schematic for the structure of an air purifier. 1—dusty gas; 2—fanner; 3—pre-filter layer; 4—core bodies; 5—ultraviolet lamp; 6—tail filter layer; 7—purified gas.

In the experiments involving formaldehyde degradation, the environment temperature was 22.7°C and the relative humidity was 30%. Each experiment was carried out in an environmental test chamber of 1 m^3 for 240 min. Two

glass-surface vessels with formaldehyde (0.267, 0.543, 0.852, 1.078, and 1.302 mg/m^3) were placed in two environmental chambers (one with an air purifier, another blank). According to the acetylacetone spectrophotometric method (standard GB/T 15516—1995), the absorbance of samples was measured at the maximum absorption wavelength of 413 nm to determine the quantity of formaldehyde. On the basis of the Lambert–Beer law, a linear relation exists between the absorbance of samples at their maximum absorption wavelength and their concentration. The removal rate for formaldehyde was calculated using the following equation:

$$\eta = \frac{A_0 - A_t}{A_0} \times 100\% \quad (1)$$

where η represents the removal rate for formaldehyde, A_0 represents the absorbance in the left chamber without an air purifier, and A_t represents the absorbance in the right chamber with an air purifier under illumination t.

3. Results and discussion

3.1. TG–DTA analysis

Fig. 2 presents the TG–DTA curves of the DBPCs coated with a nano-TiO_2 thin film after the samples were dried at 105°C. The curves show an obvious endothermic peak at 300–600°C, and the mass loss is approximately 5%. The peak is caused by an endothermic reaction of −OH groups adsorbed onto the nano-TiO_2 surface. Bacsa and Kiwi [21] reported that the DTA curve of amorphous TiO_2 powder prepared from titanium alkoxide included a strong exothermic peak at 400–500°C, which was caused by a transformation from the amorphous state to anatase. In the present research, the DTA curve of TiO_2 prepared from $TiCl_4$ did not show a similar exothermic peak, which indirectly indicated that the non-heat-treated samples were the anatase phase. The wider exothermic peak at 750–950°C in the DTA curve was likely caused by the transformation of TiO_2 from anatase to rutile. The corresponding mass loss in the TG curve is approximately 1%. The results indicate that the transformation of TiO_2 from anatase to rutile was a slow process.

3.2. Phase and structure characterization

The XRD patterns of the as-deposited samples and the samples annealed at different temperatures are shown in Fig. 3. The lower-concentration aqueous solution of titanium tetrachloride was adopted, and the reaction conditions of ammonium sulfate and ammonia were varied to control the TiO_2 crystal grain growth. The results show that the sample annealed at 650°C for 2 h was anatase TiO_2, whereas parts of the samples annealed at 750°C for 2 h transformed into rutile TiO_2.

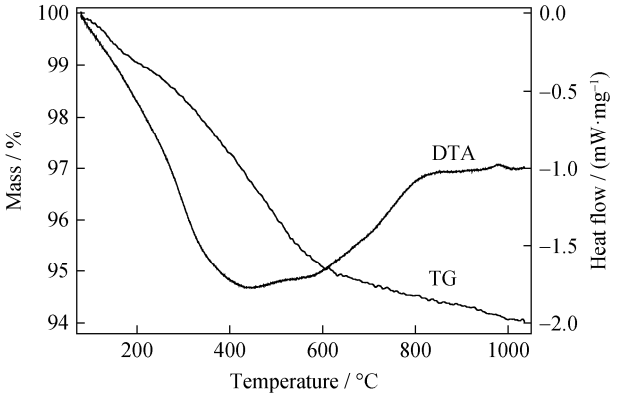

Fig. 2. TG–DTA curves of the composites.

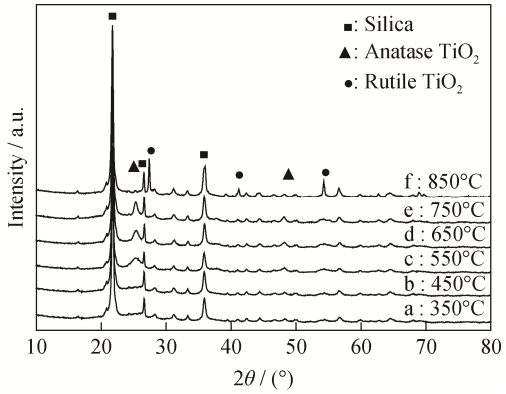

Fig. 3. XRD patterns for the annealed TiO_2 films obtained at different temperatures.

The characteristic peak of anatase TiO_2 appeared at 2θ = 25.3°. As demonstrated in the XRD patterns, no diffraction peaks of anatase TiO_2 were detected in the XRD pattern of the as-deposited thin films annealed at 350 and 450°C because the samples exhibited low crystallinity (Fig. 3(a, b)). As the annealing temperature was increased, the diffraction peaks of TiO_2 anatase appeared and became progressively narrower, indicating that the half peak width of the diffraction peaks became narrower with increasing calcination temperature and that crystallinity gradually increased (Fig. 3 (c,d,e)). After thermal treatment at 850°C for 2 h, three obvious diffraction peaks were observed (2θ = 27.4°, 41.5°, 54.3°), and the characteristic peaks of anatase TiO_2 disappeared. According to the Joint Committee on Powder Diffraction Standards (JCPDS) card PDF#84-1286 [22], these two reflections are attributed to the TiO_2 anatase phase, which shows that the anatase structure transforms into the rutile structure at higher heat-treatment temperatures. As evident from the DTA curve, the exothermic peak became more intense in the case of the sample annealed at approximately 800°C, which confirms that the transformation from anatase to rutile is a gradual process.

According to the method of XRD diffraction line width, if the crystal grain is smaller than a certain diameter, then the Debye ring widens and diffuses (full-width at half-maximum). The crystallite sizes of anatase TiO_2 can be calculated according to the Scherrer equation on the basis of the (101) peak in the XRD patterns [23]. The crystallite size of the sample prepared at 650°C was calculated to be 8.3 nm.

Fig. 4 shows the FT-IR spectra of both TiO_2 and the TiO_2 composites. As shown in Fig. 4(a), wide absorption peaks appear at 1638.27 and 3423.32 cm^{-1} because of the large number of hydroxyl groups in the matrix; peaks at these frequencies represent −OH and H−O−H bending vibrations. This result is related to the hydroxyl groups on the materials and to water adsorbed onto the surface. The peaks at 469.39, 793.23, and 1091.68 cm^{-1} are the stretching vibration absorption peaks of linear Si−O−Si formed by [SiO_4] tetrahedra. The spectrum of the as-prepared nano-TiO_2/DBPC shows weaker absorption peaks at 615.64 and 955.38 cm^{-1} in Fig. 4(b). As Ref. [23] indicates, the absorption peaks near 473–659 cm^{-1} are the vibrations of [TiO_6] and are the characteristic absorption peaks of TiO_2. The absorption peak at 955.38 cm^{-1} is attributable to the feature peaks of Ti−O−Si. According to the aforementioned analysis, new chemical bonds among Ti, O, and Si formed in the composites [24].

3.3. TEM analysis

The morphology of the TiO_2 sample treated at 650°C is presented in Fig. 5. Specifically, Fig. 5(a) shows the cross-section morphology of the matrix load of nanometric TiO_2. As evident in this image, a large number of nanoparticles are present on the surface of DBPC. The diameters of the holes on the original diatomite range from 400 to 600 nm in DBPC. The as-prepared nano-TiO_2/DBPC possesses an evident core–shell structure. The combination of the nucleus and shell is compact and the thickness of the coating layer is homogeneous (300–450 nm). As shown in Fig. 5(b), the particle diameter is approximately 10 nm, which corresponds to the XRD calculation results. The TiO_2 particle shape is near-spherical, the distribution range of particle sizes is narrow, and the spacing of particles is approximately 2–5 nm. This structure is well suited for nano-TiO_2 particles because it enables the nanoparticles to receive more radiation. This structural characteristic is important for improving the PC activity of the materials. The inset in Fig. 5(b) shows the corresponding selected-area electron diffraction pattern, and bright, clear concentric diffraction rings are observed, which further demonstrates that the as-prepared nano-TiO_2 crystal exhibits good crystallinity [15,18].

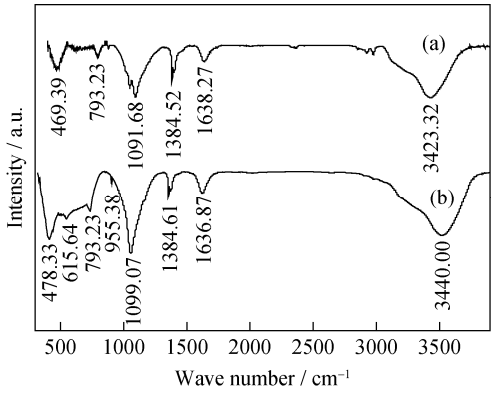

Fig. 4. FT-IR spectra of samples: (a) TiO_2; (b) nano-TiO_2/DBPC.

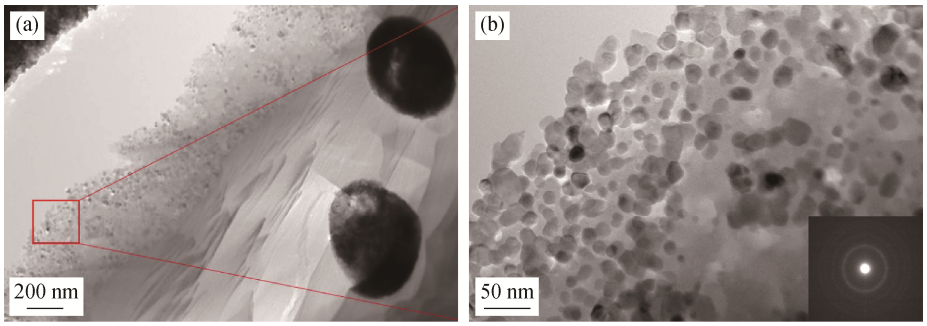

Fig. 5. TEM images of composites cross-sections (a) and the selected-area electron diffraction pattern (b).

3.4. PC degradation of formaldehyde and its dynamics analysis

Fig. 6 shows the degradation curves of formaldehyde by the composites heat-treated at different temperatures. As evident from the curves, the removal rates of formaldehyde by the samples at different temperatures for 240 min are as follows: 44.1% (350°C), 71.3% (450°C), 93.4% (550°C), 95.2% (650°C), 78.1% (750°C), and 54.5% (850°C), respectively. The results indicate that the PC performance first increases and then decreases with increasing temperature and that the sample heat-treated at 650°C exhibits the best PC performance toward the degradation of organic pollutants.

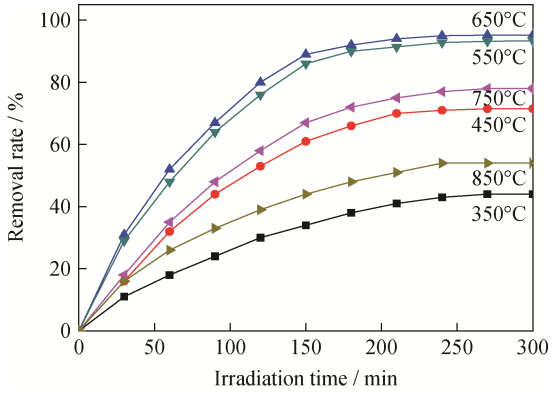

Fig. 6. Degradation curves of the samples treated at different temperatures.

The main factors influencing the PC activity of TiO_2 are the crystal structure, specific surface area, grain size, and surface characteristics. As the grain size decreases, the nanometer semiconductor particles gain a stronger redox ability to improve the PC activity with increasing quantization degree. When the particle size is smaller and the electronic diffusion time is shorter, the recombination rate of electrons and holes is smaller and the PC activity is greater.

According to the XRD patterns, anatase TiO_2 with trace quantities of rutile phase was obtained. Bickley *et al*. [25] reported that anatase TiO_2 mixed with small amounts of rutile phase exhibits greater PC activity. This greater activity was attributed to not only the "shells" hindering the ability of the "nucleus" to absorb the light, but also to the narrow band gap of rutile TiO_2 (E_g = 3.0 eV), improving the PC efficiency by making photoelectrons easily stimulated by lower-energy radiation. Therefore, the TiO_2 film heat-treated at 350 and 450°C exhibited low photocatalytic activity caused by their worse crystallinity, even though the crystal grains were small. The removal rate of formaldehyde by the sample heat-treated at 650°C was relatively higher (though the crystal grain was large), which might be related to the "mixed crystal" effect [26]. Compared with an air purifier with nano-TiO_2/ nickel-foam photocatalyst cores, the removal rate of formaldehyde increases 32.1% in the case of the same conditions. The PC oxidation process for nano-TiO_2/DBPC was studied under UV illumination. Research has shown [27] that the assumption of a pseudo-first-order model can be used to characterize the PC degradation rate of formaldehyde: $r = -\mathrm{d}c / \mathrm{d}t = \kappa Kc / (1 + Kc)$, where r is the reaction rate at some point (g·m^{-3}·min^{-1}); c is the concentration of the gas phase at some point (g·m^{-3}); κ is the reaction velocity constant for the gas phase photocatalysis as the first order reaction; K is the apparent first order reaction rate constant. This model is derivative. The relationships between the reaction time and the formaldehyde reactant concentration are shown in Fig. 7 (the formaldehyde reactant concentration was converted to molarity in this figure).

$$\frac{1}{r_0} = \frac{1}{\kappa K} \cdot \frac{1}{c_0} + \frac{1}{\kappa} \tag{2}$$

where r_0 is the beginning of the reaction starting rate (g·m^{-3}·min^{-1}); c_0 is the initial concentration of the gas phase (g·m^{-3}). $1/r_0$ and $1/c_0$ have a linear positive correlation. A line with an intercept of $1/\kappa$ and a slope of $1/(\kappa K)$ is obtained by plotting $1/c_0$ on the horizontal axis and $1/r_0$ on the vertical axis. The reaction rate constant κ and the apparent equilibrium constant K can be calculated at the same time.

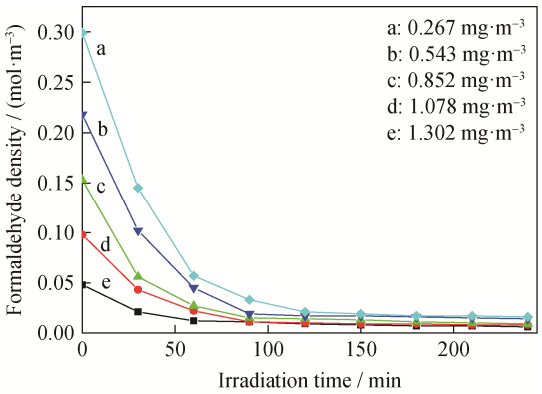

Fig. 7. Relationship between reactant concentration and reaction time at different initial concentrations of formaldehyde.

To calculate the corresponding r_0, tangents are taken at different c_0 values on the curve in Fig. 7 (as shown in Fig. 8), where the curve in Fig. 7 is a plot of $1/r_0$ as a function of $1/c_0$ [28–29]. The regression equation obtained by the least-squares linear regression correlation analysis using the experimental data is

$$\frac{1}{r_0} = 1.725 + 35.832 \frac{1}{c_0} \tag{3}$$

An excellent linear relationship of data points is observed in Fig. 8. The linear fitting variance R is as high as 0.9989. If we apply a pseudo-first-order kinetic model, then the reaction rate constants for the gas-phase PC reaction of formaldehyde are κ = 0.576 mg·m^{-3}·min^{-1} and K = 0.048 m^3/mg.

The reaction kinetics equation for the first-order gas-phase PC reaction of formaldehyde is confirmed:

$$r = -\frac{\kappa Kc}{1 + Kc} = \frac{0.0277c}{1 + 0.048c} \tag{4}$$

3.5. Catalytic stability

The stability of the nano-TiO_2/DBPC composite was evaluated through nine recycling tests. As shown in Fig. 9,

the removal rate of formaldehyde rarely decreased after nine repeated cycles. These results indicate that the composite photocatalyst exhibits stable and efficient performance for the photocatalytic degradation of formaldehyde, which is very important in practical applications.

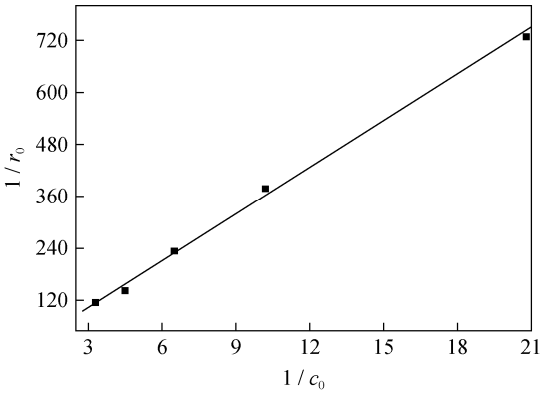

Fig. 8. Relationship between $\frac{1}{c_0}$ and $\frac{1}{r_0}$.

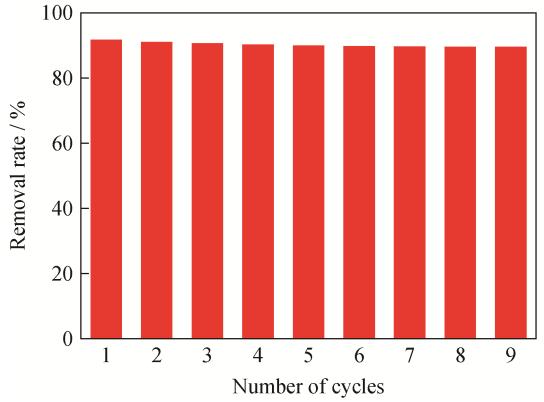

Fig. 9. Stability of the nano-TiO_2/DBPC composite toward the photocatalytic degradation of formaldehyde.

3.6. Reaction mechanism for the photodegradation of formaldehyde

Under UV irradiation, the nano-TiO_2/DBPC photocatalyst will produce photogenerated electron (e^-) and hole (h^+) pairs, which play an important role in the oxidation of formaldehyde [30]. First, formaldehyde (HCHO) and molecular oxygen (O_2) were absorbed onto the nano-TiO_2 surface [31]. Second, the absorbed O_2 accepted photoelectrons and was activated into a reactive oxygen species (O_2^-, O^-) [32–33]. Third, the absorbed HCHO was oxidized to formate ($HCOO^-$) species, which are an intermediate of HCHO during oxidation [33]. Finally, the $HCOO^-$ species were further oxidized to CO_2 and H_2O [31]. The possible reaction scheme for the photodegradation of formaldehyde is given in Eqs. (5)–(8):

$$\mathrm{HCHO+O_2+nano\text{-}TiO_2/DBPC} \xrightarrow{\text{Absorption}} \mathrm{nano\text{-}TiO_2/DBPC(HCHO,O_2)} \quad (5)$$

$$\mathrm{O_2 + e^- \rightarrow O_2^-, O^-} \quad (6)$$

$$\mathrm{HCHO + O_2^- \rightarrow HCOO^- + \cdot OH} \quad (7)$$

$$\mathrm{HCOO^- + \cdot OH + h^+ \rightarrow CO_2 + H_2O} \quad (8)$$

4. Conclusion

The nano-TiO_2 films loaded onto the surface of DBPCs by hydrolysis precipitation are the anatase phase. Their average particle size is approximately 8.3 nm after treatment at 650°C. The thickness of TiO_2 films coated onto the carrier surface is 300–450 nm. The shape of TiO_2 particles is near-spherical. The distribution range of particles is narrow, and the distance between particles is approximately 2–5 nm. When the temperature was increased to 850°C, the phase of nano-TiO_2 became rutile phase. The FT-IR spectra of the samples show the feature peaks of Ti–O–Si. Using the method of linear regression, the reaction rate constant of the gas-phase PC reaction of formaldehyde was calculated. Using the Langmuir–Hinshelwood model, we established the dynamics equation of the gas-phase PC degradation reaction of formaldehyde.

Acknowledgements

This work was financially supported by the National Natural Science Foundation of China (No. 50708037), the National Science Fund for Excellent Young Scholars of China (No. 51522402), the Science and Technology Research Projects in Zhengzhou (No. 141PPTGG388), and the National Innovation and Entrepreneurship Training Program of the Undergraduate (No. 201610078034).

References

[1] A. Fujishima, Electrochemical photolysis of water at a semiconductor electrode, *Nature*, 238(1972), No. 5358, p. 37.

[2] T.L. Thompson and J.T. Yates, Surface science studies of the photoactivation of TiO_2—new photochemical processes, *Chem. Rev.*, 106(2006), No. 10, p. 4428.

[3] C.H. Ao, S.C. Lee, Y.Z. Yu, and J.H. Xu, Photodegradation of formaldehyde by photocatalyst TiO_2: effects on the presences of NO, SO_2 and VOCs, *Appl. Catal. B*, 54(2004), No. 1, p. 41.

[4] Y.B. Xie and C.W. Yuan, Photocatalytic activity and recycle application of titanium dioxide sol for X-3B photodegradation, *J. Mol. Catal. A*, 206(2003), No. 1-2, p. 419.

[5] N. Uekawa, M. Suzuki, T. Ohmia, F. Mori, Y.J. Wu, and K. Kakegawa, Synthesis of rutile and anatase TiO_2 nanoparticles from Ti-peroxy compound aqueous solution with polyols, *J. Mater. Res.*, 18(2003), No. 4, p. 797.

[6] H. Choi, E. Stathatos, and D.D. Dionysiou, Synthesis of nanocrystalline photocatalytic TiO_2 thin films and particles using sol−gel method modified with nonionic surfactants, *Thin Solid Films*, 510(2006), No. 1-2, p. 107.

[7] A. López, D. Acosta, A.I. Martínez, and J. Santiago, Nanostructured low crystallized titanium dioxide thin films with good photocatalytic activity, *Powder Technol.*, 202(2010), No. 1-3, p. 111.

[8] X.Z. Li, H. Liu, L.F. Cheng, and H.J. Tong, Photocatalytic oxidation using a new catalyst TiO_2 microspheres for water and wastewater treatment, *Environ. Sci. Technol.*, 37(2003), No. 17, p. 3989.

[9] Q. Sun, H. Li, S.L. Zheng, and Z.M. Sun, Characterizations of nano-TiO_2/diatomite composites and their photocatalytic reduction of aqueous Cr (VI), *Appl. Surf. Sci.*, 311(2014), p. 369.

[10] S. Swati, S. Kumar, A. Umar, A. Kaur, S.K. Mehta, and S.K. Kansal, TiO_2 quantum dots for the photocatalyitc degradation of indigo carmine dye, *J. Alloys Compd.*, 650(2015), p. 193.

[11] H. Lee, M.Y. Song, J. Jurng, and Y.K. Park, The synthesis and coating process of TiO_2 nanoparticles using CVD process, *Powder Technol.*, 214(2011), No. 1, p. 64.

[12] R.Q. Gao and X.M. Hou, Preparation and photocatalytic activity of TiO_2/medical stone-based porous ceramics, *Int. J. Miner. Metall. Mater.*, 20(2013), No. 6, p. 593.

[13] S. Qiu, S.W. Xu, F. Ma, and J.X. Yang, The photocatalytic efficiency of the metal doped TiO_2 with ceramic foam as catalyst carriers, *Powder Technol.*, 210(2011), No. 2, p. 83.

[14] J.G. Wang, B. He, and X.Z. Kong, A study on the preparation of floating photocatalyst supported by hollow TiO_2 and its performance, *Appl. Surf. Sci.*, 327(2015), p. 406.

[15] T. Georgakopoulos, N. Todorova, K. Pomoni, and C. Trapalis, On the transient photoconductivity behavior of sol−gel TiO_2/ZnO composite thin films, *J. Non-Cryst. Solids*, 410(2015), p. 135.

[16] E.P. Reddy, L. Davydov, and P. Smirniotis, TiO_2-loaded zeolites and mesoporous materials in the sonophotocatalytic decomposition of aqueous organic pollutants: the role of the support, *Appl. Catal. B*, 42(2003), No. 1, p. 1.

[17] S.Y. Lu, Q.L. Wang, A.G. Buekens, J.H. Yan, X.D. Li, and K.F. Cen, Photocatalytic decomposition of gaseous 1, 2-dichlorobenzene on TiO_2 films: effect of ozone addition, *Chem. Eng. J.*, 195-196(2012), p. 233.

[18] B. Wang, G.X. Zhang, X. Leng, Z.M. Sun, and S.L. Zeng, Characterization and improved solar light activity of vanadium doped TiO_2/diatomite hybrid catalysts, *J. Hazard. Mater.*, 285(2015), p. 212.

[19] A. Šaponjić, M. Stanković, J. Majstorović, B. Matović, S. Ilić, A. Egelja, and M. Kokunešoski, Porous ceramic monoliths based on diatomite, *Ceram. Int.*, 41(2015), No. 8, p. 9745.

[20] W.W. Yuan, P. Yuan, D. Liu, W.B. Yu, L.L. Deng, and F. Chen, Novel hierarchically porous nanocomposites of diatomite-based ceramic monoliths coated with silicalite-1 nanoparticles for benzene adsorption, *Microporous Mesoporous Mater.*, 206(2015), p. 184.

[21] R.R. Bacsa and J. Kiwi, Effect of rutile phase on the photocatalytic properties of nanocrystalline titania during the degradation of *p*-coumaric acid, *Appl. Catal. B*, 16(1998), No. 1, p. 19.

[22] Q. Sun, H. Li, B.J. Niu, X.L. Hu, C.H. Xu, and S.L. Zeng, Nano-TiO_2 immobilized on diatomite: characterization and photocatalytic reactivity for Cu^{2+} removal from aqueous solution, *Procedia Eng.*, 102(2015), p. 1935.

[23] M.Z.C. Hu, M.T. Harris, and C.H. Byers, Nucleation and growth for synthesis of nanometric zirconia particles by forced hydrolysis, *J. Colloid Interface Sci.*, 198(1998), No. 1, p. 87.

[24] C. Yao, F.Q. Wu, X.P. Lin, X.J. Yang, and L.D. Lu, Study on nanosized TiO_2 coated by silica in ultrasonic field, *Chin. J. Inorg. Chem.*, 21(2005), No. 1, p. 59.

[25] R.I. Bickley, T Gonzalez-Carreno, J.S. Lees, L. Palmisano, and R.J. Tilley, A structural investigation of titanium dioxide photocatalysts, *J. Solid State Chem.*, 92(1991), No. 1, p. 178.

[26] H. Zhang, J.H. Chen, H.B. Chen, and C.J. Lin, Foaming of mixed phase nano-TiO_2 and its effect on photocatasis, *J. Mol. Catal. (China)*, 20(2006), p. 249.

[27] H. Einaga, J. Tokura, Y. Teraoka, and K. Ito, Kinetic analysis of TiO_2-catalyzed heterogeneous photocatalytic oxidation of ethylene using computational fluid dynamics, *Chem. Eng. J.*, 263(2015), p. 325.

[28] S.K. Wilkinson, I. McManus, H. Daly, J.M. Thompson, C. Hardacre, N. Sedaie Bonab, J. Ten Dam, M.J.H. Simmons, C.D'Agostino, J. McGregor, L.F. Gladden, and E.H. Stitt, A kinetic analysis methodology to elucidate the roles of metal, support and solvent for the hydrogenation of 4-phenyl-2-butanone over Pt/TiO_2, *J. Catal.*, 330(2015), p. 362.

[29] M Khairy and W Zakaria, Effect of metal-doping of TiO_2 nanoparticles on their photocatalyitc activities toward removal of organic dyes, *Egypt. J. Pet.*, 23(2014), No. 4, p. 419.

[30] Z. Wan and G. Zhang, Synthesis and facet-dependent enhanced photocatalytic activity of Bi_2SiO_5/AgI nanoplate photocatalysts, *J. Mater. Chem. A*, 3(2015), No. 32, p. 16737.

[31] Y. Ma and G. Zhang, Sepiolite nanofiber-supported platinum nanoparticle catalysts toward the catalytic oxidation of formaldehyde at ambient temperature: efficient and stable performance and mechanism, *Chem. Eng. J.*, 288(2016), p. 70.

[32] D.D. Tang and G.K. Zhang, Fabrication of $AgFeO_2$/g-C_3N_4 nanocatalyst with enhanced and stable photocatalytic performance, *Appl. Surf. Sci.*, 391(2017), p. 415.

[33] J.L. Wang, G.K. Zhang, and P.Y. Zhang, Layered birnessite-type MnO_2 with surface pits for enhanced catalytic formaldehyde oxidation activity, *J. Mater. Chem. A*, 5(2017), No. 12, p. 5719.